Physical Insights into Energy Science

Effects of Surface Transition and Adsorption on Ionic Liquid Capacitors

Huikuan Chao, and Zhen-Gang Wang

J. Phys. Chem. Lett., **Just Accepted Manuscript** • DOI: 10.1021/acs.jpclett.0c00023 • Publication Date (Web): 10 Feb 2020

Effects of Surface Transition and Adsorption on Ionic Liquid Capacitors

Huikuan Chao and Zhen-Gang Wang*

Division of Chemistry and Chemical Engineering, California Institute of Technology, Pasadena, CA 91125

E-mail: zgw@caltech.edu

Abstract

Room temperature Ionic liquids (RTILs) are synthetic electrolytes with superior electrochemical stability to conventional aqueous based electrolytes, allowing significantly enlarged electrochemical window for application as capacitors. In this study, we propose a variant of an existing RTIL model for solvent-free RTILs, accounting for both ion-ion correlations and nonelectrostatic interactions. Using this model, we explore the phenomenon of spontaneous surface charge separation in RTIL capacitors and find that this transition is a common feature for realistic choices of the model parameters in most RTILs. In addition, we investigate the effects of asymmetric preferential ion adsorption on this charge separation transition and find that proximity of the transition in this case can result in greatly enhanced energy storage. Our work suggests that differential chemical treatment of electrodes can be a simple and useful means for optimizing the energy storage in RTIL capacitors.

Ionic liquids comprise a family of salts in liquid state ranging from inorganic molten salts, molten oxides, to organic salts. In this family, room-temperature ionic liquids (RTILs), a class of synthetic organic material, have received increasing attentions in recent decades in the fields of green chemistry,[1,2] catalysis[3–5] and electronics.[6–8] Due to their superior electrochemical stability and low vapor pressure, RTILs have been utilized as supercapacitors to achieve a larger electrochemical window ($\sim 5V$).[9,10]

The promising electrochemical performance of RTIL capacitors depends on the structure of the electric double-layers near the electrodes. Because of the concentrated nature of RTILs, the classical Gouy-Chapman theory for dilute electrolytes is unable to explain the observed potential dependence of double-layer capacitance. Kornyshev[11] proposed a lattice based mean-field theory to capture the transition from camel to bell-shaped capacitance curve with increased salt concentration and the $V^{-1/2}$ decay of the capacitance at high potentials, that are observed both in experiments[12,13] and in computer simulations.[14–16] To account for electrostatic correlation effects beyond the mean-field level, Bazant, Storey and Konyshev (BSK),[17] constructed a phenomenological field theory by including non-locality in permittivity in a Ginzburg-Landau type expansion. The theory predicts overscreening of the surface charge at low potentials and crowing of counterions at high potentials, consistent with simulation results on capacitance[18] and experimental observations on the structure of the RTIL double-layer.[19,20]

Experimentally measured capacitance in RTILs often exhibit hysteresis when charging direction is reversed.[21,22] Motobayashi et al.[23] and Uysal et al.[24] suggested that the hysteresis was due to slow dynamics in the restructuring of RTIL double-layers during charging/uncharging processes. Another possible explanation is that hysteresis is a manifestation of an underlying phase transition. Lee and Perkin proposed a phenomenological model of RTIL with implicit solvents[25] by considering image charge interactions in the RTIL immediate to the metal electrodes, which predicts a first-order transition in the total ion concentration in the proximate RTIL layer induced by finite potential differences. However, the

theory does not anticipate a transition for solvent-free RTILs where hysteresis was nevertheless observed experimentally.[21,22] An alternative phenomenological model was proposed by Limmer[26] which adds a repulsive nonelectrostatic interaction between the opposite charges in addition to the Coulomb interactions. Both a mean-field analysis and Monte Carlo simulation reveal a surface charge-separation transition which takes place prior to any bulk phase transition. However, in his analysis, the applied surface potential is treated as an effective preferential adsorption to one of the ionic species, which is only valid in the linear response regime and is incapable of describing the effects of a true preferential adsorption in the presence of finite applied potentials. In addition, the physical origin of the repulsive nonelectrostatic interaction and its connection to the ion-ion correlations in real RTILs are not clear.

In this Letter, we propose a variant of the BSK model for solvent-free RTILs that includes both ion-ion correlations and nonelectrostatic interactions. We then use this model to study the spontaneous charge separation transition near the surface and its consequence on the capacitance behavior. We find that this transition is a common feature for realistic choices of the model parameters for most RTILs. Furthermore, we examine the effects of preferential ion adsorption on this charge separation transition, which can be a useful design parameter for optimizing the performance of the capacitors.

We start with the BSK model for a solvent-free RTIL consisting of a symmetric mixture of cations and anions that carry the unit charge, $\pm e$, the same unit size, b, and the same molecular volume, v. The Helmholtz free energy is,

$$\begin{aligned}\beta\mathcal{F} &= \frac{1}{v}\int d\mathbf{r}\left[\frac{1+\phi}{2}\ln\left(\frac{1+\phi}{2}\right)+\frac{1-\phi}{2}\ln\left(\frac{1-\phi}{2}\right)\right] \\ &\quad +\frac{1}{v}\int d\mathbf{r}\left\{\phi\psi-\lambda_D^2\left[|\nabla\psi|^2+l_c^2(\nabla^2\psi)^2\right]\right\}, \qquad (1)\end{aligned}$$

where ϕ is the local dimensionless charge density, which serves as an order parameter for our system, ψ is the electrostatic potential nondimensionalized by k_BT/e, and λ_D is the

(nominal) screening length defined as $\lambda_D = [\epsilon v/(2\beta e^2)]^{1/2}$, with ϵ being the permittivity. In the absence of the last term, the two terms in the second line of the equation represents the usual Coulomb interaction for the mean charge density. The last term $-\lambda_D^2 l_c^2 (\nabla^2\psi)^2$ accounts for the strong electrostatic correlations in RTIL, with l_c^2 a measure of the strength of the correlation. In the BSK formulation, this term is interpreted as adding a wavenumber dependence to the dielectric function, which leads to a modification of the Poisson equation.

We now provide a reformulation of the BSK free energy in the following way. As pointed out by de Souza and Bazant,[27] the effect of the correlation is to change the bare Coulomb interaction into an effective interaction of the following form $U_{eff}(\mathbf{r}) = \frac{1}{4\pi\lambda_D^2 r}\left(1 - \alpha e^{-r/l_c}\right)$, where we have included an additional dimensionless parameter, α, to control the strength of the correlation (vide infra); the original BSK model corresponds to $\alpha = 1$. Note that the second (Yukawa) term can also arise from some short-ranged effective repulsion between the anions and cations, as in the model used in Limmer's work.[26] Thus, this term can account for both electrostatic correlations and some short-ranged nonelectrostatic interactions. Here, for simplicity, we assume these two types of interaction are of the same range, and use the parameter α to control their total strength. Note that the use of a single parameter in the interaction for the charge density, rather than three for the cation-cation, anion-anion and cation-anion, respectively, is due to the incompressibility of the ionic liquid. The interaction part of the free energy can now be written as

$$\begin{aligned} \beta\mathcal{F}_{int} &= \frac{1}{8\pi\lambda_D^2 v}\int d\mathbf{r}\int d\mathbf{r}'\frac{\phi(\mathbf{r})\phi(\mathbf{r}')}{|\mathbf{r}-\mathbf{r}'|} \\ &- \frac{\alpha}{8\pi\lambda_D^2 v}\int d\mathbf{r}\int d\mathbf{r}'\frac{\phi(\mathbf{r})e^{-|\mathbf{r}-\mathbf{r}'|/l_c}\phi(\mathbf{r}')}{|\mathbf{r}-\mathbf{r}'|}. \end{aligned} \tag{2}$$

Within the random phase approximation, the charge-density structure factor for our free energy model is $S(\mathbf{k}) = \left[1 + \frac{l_c^2}{2\lambda_D^2}\left(\frac{1}{l_c^2 k^2} - \frac{\alpha}{1+l_c^2 k^2}\right)\right]^{-1}$, which is in agreement with that from BSK model when $\alpha = 1$. However, the BSK structure factor lacks a peak at intermediate values of k, which is only obtained for $\alpha > 1$ and is a typical feature for solvent-free RTILs.[28,29]

We thus allow α to take values beyond unity in order to capture this important structural property.

Since the second term in Eq. 2 arises from correlation effects and other short-range interactions, the presence of fixed external charges should not affect this term. Any additional charge density from fixed external sources will only add to the charge density in the first, Coulomb term. Introducing the electrostatic potential ψ, the first Coulomb term of Eq. 2 becomes simply the first two terms in the second line of Eq. 1. We decouple the bilinear Yukawa interaction using a similar strategy by introducing another auxiliary field Y. Specifying to our model of the capacitor as an RTIL between two planar metal surfaces separated by a distance L, the interaction free energy is transformed to

$$\beta\mathcal{F}_{int} = \frac{1}{v}\int d\mathbf{r}\left[\phi Y + \left[\phi - \sigma\delta(z) + \sigma\delta(z-L)\right]\psi - \lambda_D^2|\nabla\psi|^2 + \frac{\lambda_D^2}{\alpha}\left(|\nabla Y|^2 + Y^2/l_c^2\right)\right], \quad (3)$$

where σ and $-\sigma$ are the charge densities scaled by e/v on the two surfaces. Variation of the free energy with respect to the two potential fields ψ and Y yields, $\phi - \sigma\delta(z) + \sigma\delta(z-L) = -2\lambda_D^2\nabla^2\psi$, and $\phi = 2\alpha^{-1}\lambda_D^2(\nabla^2 Y - Y/l_c^2)$, respectively. We note that the first condition is just the Poisson equation. Importantly, these two equations naturally yield the boundary conditions, $2\lambda_D^2\nabla\psi|_S = \sigma$ and $\nabla Y|_S = 0$, upon integrating z over an infinitesimal width across each boundary. Together with the variational condition $\delta\mathcal{F}/\delta\phi = 0$, we can now solve for the three fields self-consistently.

To allow for preferential adsorption of ions on the electrodes, we add a coupling term $-h_i\phi$ to each surface, where h_i is the adsorption strength. For numerical stability and to be consistent with the length scale of the description of the RTIL, we let the adsorption potential assume the form of a half-sided harmonic potential of the form, $-\frac{A}{v}\int_0^a dz\frac{(a-z)^2}{a^2}\left[h_1\phi(z) + h_2\phi(L-z)\right]$, where A is the surface area and a is the interaction range which is of the order of the ion size.

Since the controlling variable in capacitor applications is typically the voltage, rather

than the surface charge, we construct the Gibbs free energy by

$$\beta\mathcal{G} = \beta\mathcal{F} - \frac{A}{v}\Delta V\sigma. \tag{4}$$

The surface charge is then obtained by variation of $\mathcal{G}$ with respect to σ.

The structure factor for our model has a peak located at $k^* = l_c^{-1}\left(\alpha^{1/2} - 1\right)^{-1/2}$; the divergence of the structure at this position gives a spinodal value for the parameter $\alpha_c = 2(\lambda_D/l_c)^2 + 2^{3/2}(\lambda_D/l_c) + 1$. Because of the symmetry of the free energy in ϕ, the transition is second order at the mean-field level but becomes weakly first order due to fluctuation effects.[30] We will limit our analysis to mean-field in this work. Performing a linear stability analysis for a decaying oscillatory charge density profile near the surface, we find that the profile becomes unstable at a critical value of $\alpha_{s,c} = 2(\lambda_D/l_c)^2 + \sqrt{2}(\lambda_D/l_c)$ (see SI); this signals a spontaneous surface charge separation at zero potential difference. This means that the cathode and the anode in a closed circuit will spontaneously acquire the same amount of opposite surface charge while the ionic liquid as a whole remains charge neutral. Note that $\alpha_{s,c} < \alpha_c$; this result is consistent with that obtained by Limmer.[26] The bulk and surface critical values of α are shown in Fig. 2a. We also note that for ionic liquids with $\alpha = 1$ and λ_D/l_c in the range between 0 and 0.42, the model predicts a surface charge separation transition even though the bulk structure factor does not possess a peak at intermediate wavenumbers. To see where real ionic liquids are located on the phase diagram, we fit our model parameters using the $S(\mathbf{k})$ data at intermediate values of k from molecular dynamics simulations[28,29,31,32] for three ionic liquids: molten NaCl and two imidazolium-based RTILs (see SI). As pointed out by BSK,[17] the correlation length l_c is on the order of the ion sizes, so we set $l_c = b$ in our fitting. The fitting results show that all three ionic liquids are located in the region where there is spontaneous surface charge separation but where the bulk remains stable (Fig. 1a). This is quite remarkable given the large variations in both the physical condition ($T \sim 1300K$ to $\sim 300K$) and chemical nature (inorganic and organic) among

these ionic liquids. The fitted αs are found to be larger than one and well beyond the surface transition value ($\alpha/\alpha_{s,c} \sim 6$). This result suggests that spontaneous charge separation is a common feature for ionic liquids capacitors.

Phenomenologically, the spontaneous surface charge separation is similar to the spontaneous magnetization in a mean-field Ising model if we take the surface charge density as the order parameter. Fig. 1b shows the magnitude of the surface charge density in the absence of applied voltage for an RTIL with $\lambda_D/b = 0.1$ (corresponding to the two imidazolium-based RTILs modeled here); the $\sigma = 0$ solution bifurcates at $\alpha_{s,c}$ and becomes nonzero for $\alpha > \alpha_{s,c}$ (the figure only shows the $\sigma > 0$ half of the diagram.) The corresponding charge density in the surface-charge-separated state develops an oscillatory profile where the first layer of counter-ions over-screens the surface charge;[17] see the inset of Fig. 1b. In Fig. 1c, we show the "equation of state"(EOS) – the σ–ΔV relationship for α between 0 and 1.1. The slope in the σ – ΔV curve is the differential capacitance $C = \frac{\partial \sigma}{\partial \Delta V}$. As expected for any mean-field critical point, the capacitance diverges at $\alpha_{s,c}$ for $\Delta V = 0$. Beyond $\alpha_{s,c}$, each branch of the curve develops a metastable part that starts from the coexistence point at $\Delta V = 0$ and expands with increasing α. The existence of such metastable states could be responsible for the observed hysteresis in the measured capacitance upon reversal of the charging direction. At large ΔV on the stable branch, the capacitance decays as $\Delta V^{-1/2}$, consistent with Kornyshev's prediction.[11] For the fitted values of α for the imidazolium-based RTILs above, the metastable region can span a large range of the ΔV ($1.5V$ in real units), comparable to the electrochemical window for typical RTIL capacitors. Since hysteresis in general results in uncontrolled energy dissipation, spontaneous surface charge separation is usually undesirable for capacitance applications.

For $\alpha < \alpha_{s,c}$, the capacitance exhibits a peak at $\Delta V = 0$, with a peak height increasing as $\alpha \to \alpha_{s,c}$; however, the width of the peak (shown as a shoulder or plateau in Fig. 1d) decreases. Consequently, not much is gained in terms of the total electric energy storage due to proximity to the surface charge separation transition.

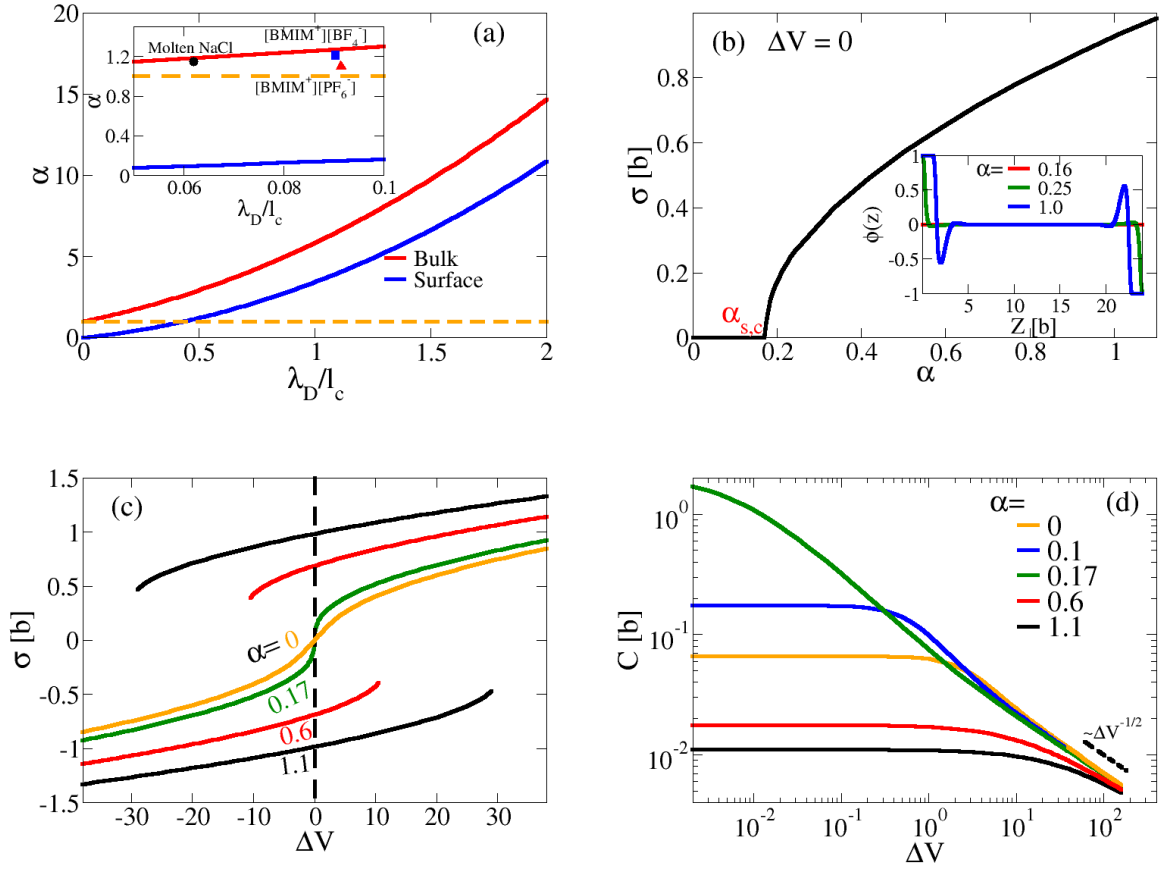

Figure 1: (a) Phase digram of ionic liquids, where the spontaneous surface charge separation is predicted between the bulk (α_c, red line) and surface ($\alpha_{s,c}$, blue line) critical lines. The inset shows the locations of three ionic liquids, molten NaCl (black dot) , $[\mathrm{BMIM}^+][\mathrm{BF}_4^-]$ (blue square), and $[\mathrm{BMIM}^+][\mathrm{PF}_6^-]$ (red triangle) in the diagram. (b) Surface charge density, σ, as a function of α for $\Delta V = 0$. The inset shows charge density profiles at selected values of α. (c) σ as a function of ΔV at different values of α. (d) Differential capacitance (C) as a function of the applied potential difference, ΔV. Different colors corresponds to different values of α. In (b), (c), and (d) λ_D/b and v/b^3 are set to 0.1 and 1.0 for the calculations, respectively.

However, if the capacitance peak is shifted to a finite ΔV^* due to asymmetry in the system, then proximity to the surface transition can greatly increase the energy storage. This is because the free energy change upon charging to ΔV is

$$\beta \Delta F = \frac{A}{v} \int_{\sigma(0)}^{\sigma(\Delta V)} u d\sigma(u) = \frac{A}{v} \int_0^{\Delta V} C u du \tag{5}$$

Thus, if C has a sharp peak at ΔV^*, then as ΔV is increased across ΔV^*, the spike in the integrand Cu will give rise to a sharp increment to the integral and hence the stored energy.

We propose that surface adsorption asymmetry between the two electrodes can result in a finite ΔV^* at the surface transition. To demonstrate this, we consider the simplest case where one surface, say the cathode, has a preferential adsorption for the cations with an adsorption strength $h > 0$, while the other surface is indifferent, i.e. $h = 0$. (Making the anode attractive to anions will obviously further enhance the effect.) The asymmetry between the electrodes results in a finite surface charge even in the absence of applied voltage ($\Delta V = 0$). However, a surface transition still exists for large enough α, but now the transition occurs at finite ΔV (see SI for the EOS). The critical $\alpha_{s,c}$ and $\Delta V_{s,c}$ depend on the adsorption strength h (Fig. 3 in SI). At the critical point, the susceptibility – the capacitance – diverges as shown by the green curve in Fig. 2a. This sharp capacitance peak leads to a sharp increase in the energy storage when charging the system beyond $\Delta V_{s,c}$. Even when α is only half its critical value, there is still significantly enhanced energy storage (blue solid curve) compared to the symmetric case at its critical α (black dashed line) beyond the location of the capacitance peak in ΔV.

We note that a shifted capacitance peak at finite voltage has been reported in previous work for different anion and cation sizes at a single surface.[33,34] However, such size asymmetry, or any other asymmetry, will not lead to a net shifted capacitance peak at finite voltage for capacitors with indentical surface (electrode) properties. There needs to be asymmetry in the two electrodes in order to produce a shifted capacitance peak at finite voltage for the

capacitor.

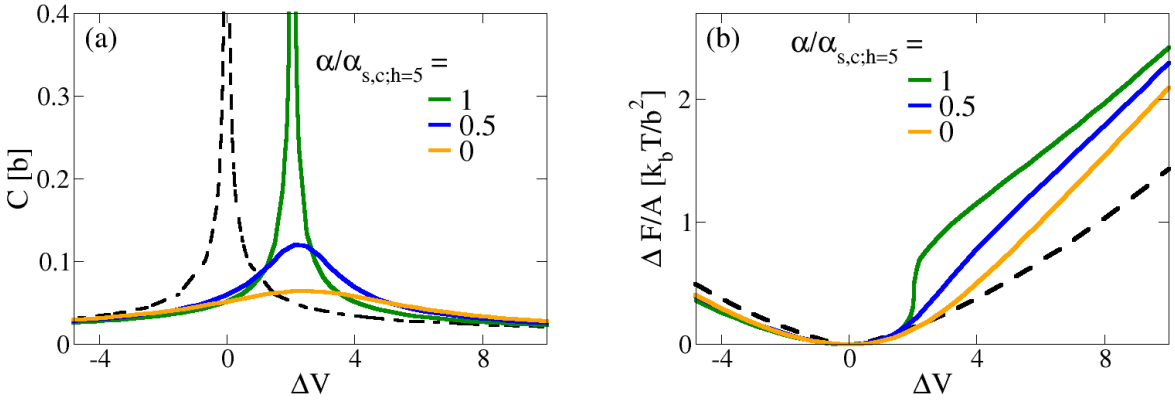

Figure 2: (a) Capacitance (C) as a function of the applied potential difference, ΔV with the adsorption asymmetry, $h_1 = 0,\ h_2 = h = 5$. The different colors here correspond to different values of α. The dashed line shows the results from the adsorption-free case. (b) Free energy storage, ΔF as a function of ΔV with the same color scheme and line style as in (a).

Increasing the adsorption strength h shifts the position of the capacitance peak toward more positive ΔV. In Fig 3a, we show the capacitance peaks for three different values of h, all at the adsorption-free critical value $\alpha_{s,c}$. With the shift of the peak towards larger ΔV, we obtain higher energy storage, albeit at higher applied potential; see Fig 3b.

At a given working potential, there is an optimal adsorption strength that gives the maximum energy storage. In Fig 4, we show a heat map of the energy storage as a function of h and α at $\Delta V = 4$ ($\sim 0.1V$ in real units). The maximum energy storage shifts toward larger h and shows increasing magnitude, as α approaches its critical value for the adsorption-free .

In conclusion, we have shown using a modified BSK model with reasonable parameters for real ionic liquids that surface transition is a common feature for many ionic liquids including RTILs such as imidazolium-based ionic liquids. This transition results in the appearance of metastable branches in the $\sigma - \Delta V$ relationship, which could be responsible for the observed hysteresis in the capacitance measurements when the charging direction is reversed. Since this transition arises from an effective attraction between like charges (or equivalently

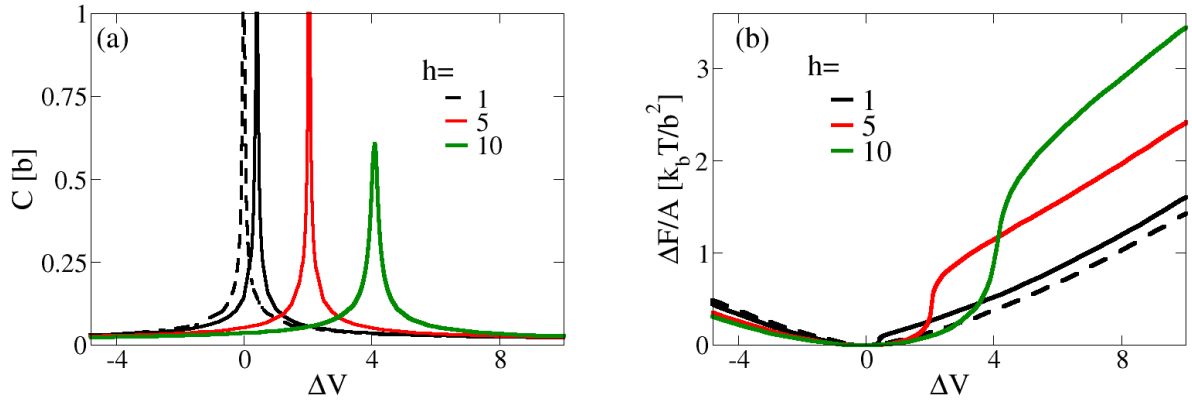

Figure 3: (a) Capacitance (C) as a function of the applied potential difference, ΔV for $\alpha = \alpha_{s,c;h=0}$ with the adsorption asymmetry $h_1 = 0,\ h_2 = h$. The different colors correspond to the values of $h = 1,\ 5,\ 10$. The dashed line shows the results from the adsorption-free case. (b) Free energy storage, ΔF as a function of ΔV with the same color scheme and line style as in (a).

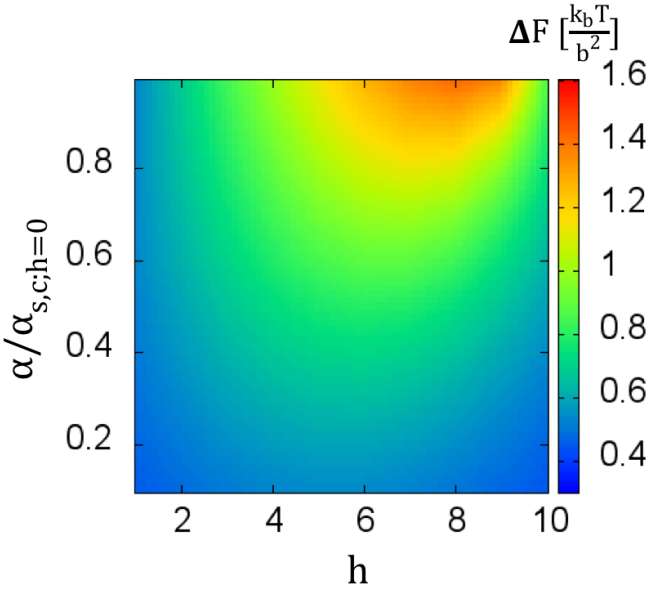

Figure 4: Heat map of the energy storage as a function of the adsorption asymmetry h and the strength of the correlation α relative to the adsorption-free critical value at the applied potential difference $\Delta V = 4$.

effective repulsion between opposite charges), which can either be due to electrostatic correlations, or effective repulsion between the anions and cations due to their chemical differences, to avoid the hysteresis, one needs to reduce the strength of electrostatic correlations or de-

crease the chemical incompatibility between the anion and the cation, through, for example, the addition of a solvent. We have also shown that asymmetric preferential adsorption of ions between the the cathode and the anode can lead to enhanced energy storage due to the shift of the capacitance peak to finite voltage. Preferential adsorption naturally exists in many RTILs. For example, many metallic surfaces have a preferential affinity to the imidazolium-based cations.[35–37] Our study suggests to use different metal surfaces for the two electrodes or to chemically modify the surfaces so the two electrodes have large affinity contrast towards the cations and anions. The enhancement of the energy storage is most pronounced at the critical point. Thus an optimal system design is such that α is close to but below the critical value for the surface transition. Experimental studies to test some of the predictions given here would be most welcome. Atomistic simulations that capture the specific chemistries and structures of the cations and anions, and their interactions with each other and with the electrodes, would also provide more direct test of the current theory and connect the parameters in the phenomenological theory to molecular properties.

References

(1) Rogers, R. D.; Seddon, K. R. Perspective Article: Ionic Liquids Solvents of the Future? *Science* **2003**, *302*, 792–793.

(2) Moniruzzaman, M.; Goto, M. Ionic liquids: Future Solvents and Reagents for Pharmaceuticals. *J Chem. Eng. Jpn.* **2011**, *44*, 370–381.

(3) Pârvulescu, V. I.; Hardacre, C. Catalysis in Ionic Liquids. *Chem. Rev.* **2007**, *107*, 2615–2665.

(4) Sheldon, R. Catalytic Reactions in Ionic Liquids. *Chem. Commun.* **2001**, 2399–2407.

(5) Zhao, D.; Wu, M.; Kou, Y.; Min, E. Ionic liquids: Applications in Catalysis. *Catal.* **2002**, *74*, 157–189.

(6) Lu, W.; Fadeev, A. G.; Qi, B.; Smela, E.; Mattes, B. R.; Ding, J.; Spinks, G. M.; Mazurkiewicz, J.; Zhou, D.; Wallace, G. G. et al. Use of Ionic Liquids for π-conjugated Polymer Electrochemical Devices. *Science* **2002**, *297*, 983–987.

(7) Balducci, A.; Bardi, U.; Caporali, S.; Mastragostino, M.; Soavi, F. Ionic Liquids for Hybrid Supercapacitors. *Electrochem. commun.* **2004**, *6*, 566–570.

(8) Kim, T. Y.; Lee, H. W.; Stoller, M.; Dreyer, D. R.; Bielawski, C. W.; Ruoff, R. S.; Suh, K. S. High-Performance Supercapacitors Based on Poly(Ionic Liquid)-Modified Graphene Electrodes. *ACS Nano* **2011**, *5*, 436–442.

(9) Arbizzani, C.; Biso, M.; Cericola, D.; Lazzari, M.; Soavi, F.; Mastragostino, M. Safe, High-Energy Supercapacitors Based on Solvent-Free Ionic Liquid Electrolytes. *J. Power Sources* **2008**, *185*, 1575–1579.

(10) Mousavi, M. P.; Wilson, B. E.; Kashefolgheta, S.; Anderson, E. L.; He, S.; Bühlmann, P.; Stein, A. Ionic Liquids as Electrolytes for Electrochemical Double-Layer Capacitors: Structures that Optimize Specific Energy. *ACS Appl. Mater. Interfaces* **2016**, *8*, 3396–3406.

(11) Kornyshev, A. A. Double-Layer in Ionic Liquids: Paradigm Change? *J Phys. Chem. B* **2007**, *111*, 5545–5557.

(12) Islam, M. M.; Alam, M. T.; Ohsaka, T. Electrical Double-Layer Structure in Ionic Liquids: a Corroboration of the Theoretical Model by Experimental Results. *J Phys. Chem. C* **2008**, *112*, 16568–16574.

(13) Lockett, V.; Sedev, R.; Ralston, J.; Horne, M.; Rodopoulos, T. Differential Capacitance of the Electrical Double Layer in Imidazolium-Based Ionic Liquids: Influence of Potential, Cation Size, and Temperature. *J Phys. Chem. C* **2008**, *112*, 7486–7495.

(14) Fedorov, M. V.; Kornyshev, A. A. Ionic Liquid Near a Charged Wall: Structure and Capacitance of Electrical Double Layer. *J Phys. Chem. B* **2008**, *112*, 11868–11872.

(15) Nakayama, Y.; Andelman, D. Differential Capacitance of the Electric Double Layer: the Interplay Between Ion Finite Size and Dielectric Decrement. *J Chem. Phys.* **2015**, *142*, 044706.

(16) Chen, M.; Goodwin, Z. A.; Feng, G.; Kornyshev, A. A. on the Temperature Dependence of the Double Layer Capacitance of Ionic Liquids. *J. Electroanal. Chem.* **2018**, *819*, 347–358.

(17) Bazant, M. Z.; Storey, B. D.; Kornyshev, A. A. Double Layer in Ionic Liquids: Overscreening versus Crowding. *Phys. Rev. Lett.* **2011**, *106*.

(18) Fedorov, M. V.; Kornyshev, A. A. Towards Understanding the Structure and Capacitance of Electrical Double Layer in Ionic Liquids. *Electrochim. Acta* **2008**, *53*, 6835–6840.

(19) Zhong, Y. X.; Yan, J. W.; Li, M. G.; Zhang, X.; He, D. W.; Mao, B. W. Resolving Fine Structures of the Electric Double Layer of Electrochemical Interfaces in Ionic Liquids with an AFM Tip Modification Strategy. *J. Am. Chem. Soc.* **2014**, *136*, 14682–14685.

(20) Li, M.-G.; Chen, L.; Zhong, Y.-X.; Chen, Z.-B.; Yan, J.-W.; Mao, B.-W. the Electrochemical Interface of Ag(111) in 1-Ethyl-3-Methylimidazolium bis(Trifluoromethylsulfonyl)Imide Ionic Liquid–A Combined In-Situ Scanning Probe Microscopy and Impedance Study. *Electrochim. Acta* **2016**, *197*, 282–289.

(21) Zhou, W.; Inoue, S.; Iwahashi, T.; Kanai, K.; Seki, K.; Miyamae, T.; Kim, D.; Katayama, Y.; Ouchi, Y. Double Layer Structure and Adsorption/Desorption Hysteresis of Neat Ionic Liquid on Pt Electrode Surface - an In-Situ IR-Visible Sum-Frequency Generation Spectroscopic Study. *Electrochem. Commun.* **2010**, *12*, 672–675.

(22) Drüschler, M.; Huber, B.; Passerini, S.; Roling, B. Hysteresis Effects in the Potential-Dependent Double Layer Capacitance of Room Temperature Ionic Liquids at a Polycrystalline Platinum Interface. *J Phys. Chem. C* **2010**, *114*, 3614–3617.

(23) Motobayashi, K.; Minami, K.; Nishi, N.; Sakka, T.; Osawa, M. Hysteresis of Potential-Dependent Changes in Ion Density and Structure of an Ionic Liquid on a Gold Electrode: In Situ Observation by Surface-Enhanced Infrared Absorption Spectroscopy. *J Phys. Chem. Lett.* **2013**, *4*, 3110–3114.

(24) Uysal, A.; Zhou, H.; Feng, G.; Lee, S. S.; Li, S.; Fenter, P.; Cummings, P. T.; Fulvio, P. F.; Dai, S.; McDonough, J. K. et al. Structural Origins of Potential Dependent Hysteresis at the Electrified Graphene/Ionic Liquid Interface. *J Phys. Chem. C* **2014**, *118*, 569–574.

(25) Lee, A. A.; Perkin, S. Ion-Image Interactions and Phase Transition at Electrolyte-Metal Interfaces. *J Phys. Chem. Lett.* **2016**, *7*, 2753–2757.

(26) Limmer, D. T. Interfacial Ordering and Accompanying Divergent Capacitance at Ionic Liquid-Metal Interfaces. *Phys. Rev. Lett.* **2015**, *115*, 256102.

(27) de Souza, J. P.; Bazant, M. Z. Continuum Theory of Electrostatic Correlations at Charged Surfaces. 2019; arXiv:1902.05493 [cond-mat.soft].

(28) McDaniel, J. G.; Yethiraj, A. Influence of Electronic Polarization on the Structure of Ionic Liquids. *J Phys. Chem. Lett.* **2018**, *9*, 4765–4770.

(29) McDaniel, J. G.; Yethiraj, A. Understanding the Properties of Ionic Liquids: Electrostatics, Structure Factors, and Their Sum Rules. *J Phys. Chem. B* **2019**, *123*, 3499–3512.

(30) Brazovskii, S. A. Phase Transition of an Isotropic System to a Nonuniform State. *Zh. Eksp. Teor. Fiz.* **1975**, *68*, 175, [English translation: *Sov. Phys. JETP* **41**, 85, (1975)].

(31) Hansen, J.; McDonald, I. *Theory of Simple Liquids*; Academic Press, 1990.

(32) Hansen, J. P.; McDonald, I. R. Statistical Mechanics of Dense Ionized Matter. IV. Density and Charge Fluctuations in a Simple Molten Salt. *Phys. Rev. A* **1975**, *11*, 2111–2123.

(33) Jiang, D. E.; Meng, D.; Wu, J. Density Functional Theory for Differential Capacitance of Planar Electric Double Layers in Ionic Liquids. *Chem. Phys. Lett.* **2011**, *504*, 153–158.

(34) Ma, K.; Woodward, C. E.; Forsman, J. Classical Density Functional Study on Interfacial Structure and Differential Capacitance of Ionic Liquids Near Charged Surfaces. *J Phys. Chem. C* **2014**, *118*, 15825–15834.

(35) Lin, L. G.; Wang, Y.; Yan, J. W.; Yuan, Y. Z.; Xiang, J.; Mao, B. W. an In Situ STM Study on the Long-Range Surface Restructuring of Au(111) in a Non-Chloroaluminumated Ionic Liquid. *Electrochem. Commun.* **2003**, *5*, 995–999.

(36) Mezger, M.; Schröder, H.; Reichert, H.; Schramm, S.; Okasinski, J. S.; Schöder, S.; Honkimäki, V.; Deutsch, M.; Ocko, B. M.; Ralston, J. et al. Molecular Layering of Fluorinated Ionic Liquids at a Charged Sapphire (0001) Surface. *Science* **2008**, *322*, 424–428.

(37) Yan, J. W.; Tian, Z. Q.; Mao, B. W. Molecular-Level Understanding of Electric Double Layer in Ionic Liquids. *Curr. Opin. Electrochem.* **2017**, *4*, 105–111.

Graphical TOC Entry